TASK QUARTERLY 15 No 3–4, 251–270

SOLUTION OF THE DIKE-BREAK PROBLEM USING FINITE VOLUME METHOD AND SPLITTING TECHNIQUE

DARIUSZ GĄSIOROWSKI

Faculty of Civil and Environmental Engineering,
Gdansk University of Technology,
Narutowicza 11/12, Gdansk 80-233, Poland
gadar@pg.gda.pl

(Received 6 June 2011; revised manuscript received 13 August 2011)

Abstract: In this paper, an approach using the finite volume method (FVM) for the solution of two-dimensional shallow water equations is described. Such equations are frequently used to simulate dam-break and dike-break induced flows. The applied numerical algorithm of the FVM is based on a wave-propagation algorithm, which ensures a stable solution and, simultaneously, minimizes numerical errors. Dimensional decomposition according to the coordinate directions was used to split two-dimensional shallow water equations into one-dimensional equations. Additionally, splitting was also applied with respect to the physical processes. The applied dimensional and physical splitting, together with the wave-propagation algorithm led to an effective algorithm and ensured proper incorporation of source terms into the scheme of the finite volume method. A detailed description of an approximation for numerical fluxes and source terms is presented. The obtained numerical results are compared with analytical solutions, laboratory experiments and other results available in the literature.

Keywords: finite volume method, shallow water equations, approximate Riemann solver, dam-break, dike-break, wave-propagation method

1. Introduction

Unsteady flow in rivers, shallow reservoirs and flood plains can be simulated by means of the shallow water equations (SWEs). In order to solve these equations, the finite difference or finite element methods are frequently used [1–3]. These methods give highly accurate solutions for gradually varied flow. However, the use of standard numerical methods leads to inaccurate and unstable solutions for flows with a discontinuity, which can arise during dam-break or dike-break induced flows. In such a case, unphysical oscillations or significant attenuation of the wave are observed in the numerical solution. These unphysical effects result from numerical dispersion and diffusion, which are introduced into the solution. In order

to overcome these problems, the shallow water equations should be written in their appropriate conservative form and solved by means of finite volume methods. Numerical schemes for finite volume methods are based on the wave structure of the approximate solution of the Riemann problem. These methods were originally used in gas dynamics for the Euler equations [4, 5]. Such an approach has been also applied in hydrodynamics to the solution of the shallow water equations in order to simulate dam-break problems for one-dimensional flow [6, 7] and two-dimensional flow [8–10], as well as to simulate dike-break induced flow [11–13].

In this paper, the solutions of one- and two-dimensional shallow water equations are presented. The numerical algorithm of the finite volume method was based on the wave-propagation algorithm proposed by LeVeque [5, 14]. In order to obtain an efficient algorithm, directional decomposition of a two-dimensional system was used. As a result, the solution of the two-dimensional problem was reduced to the solution of a sequence of one-dimensional problems.

Correct approximation of the source terms, which represent both variable bottom slope and friction, is crucial when solving the shallow water equations by the finite volume method. For the approximation of the bottom source term, flux-based wave decomposition [15] was used, whereas for the friction source term, splitting with respect to the physical processes is proposed. This type of splitting algorithm, presented by Szymkiewicz [16] in accordance with the solution of the SWEs by the finite difference method, seems to be suitable for the considered problem. In this paper, this method of approximating the friction source term was adopted for the wave-propagation algorithm.

The paper is organized as follows. First, the one-dimensional problem for a homogeneous system of equations without a source term is considered. Then, a system which incorporates the source term associated with a variable bottom and a source term due to friction are analyzed. A detailed description of an approximation for each term is presented. The method was applied to the two-dimensional shallow water equations for dam-break and dike-break problems. For the one-dimensional case, the numerical results were compared with the existing analytical solution. The numerical solutions of the two-dimensional dam-break and dike-break induced flow were compared with the numerical and laboratory experiments available in the literature.

2. Shallow water equations

The shallow water equations are comprised of the continuity and dynamic equations, which are derived from the conservation laws of mass and momentum, respectively [2]. The two-dimensional depth-integrated shallow water equations in the conservation form can be written as:

$$\frac{\partial \boldsymbol{U}}{\partial t} + \frac{\partial \boldsymbol{F}}{\partial x} + \frac{\partial \boldsymbol{G}}{\partial y} = \boldsymbol{S}_{0x} + \boldsymbol{S}_{0y} + \boldsymbol{S}_{fx} + \boldsymbol{S}_{fy} \tag{1}$$

with:

$$\boldsymbol{U}=\begin{bmatrix} h \\ u\cdot h \\ v\cdot h \end{bmatrix}, \quad \boldsymbol{F}=\begin{bmatrix} u\cdot h \\ u^2h+0.5g\cdot h^2 \\ u\cdot v\cdot h \end{bmatrix}, \quad \boldsymbol{G}=\begin{bmatrix} v\cdot h \\ u\cdot v\cdot h \\ v^2h+0.5g\cdot h^2 \end{bmatrix} \tag{2}$$

$$\boldsymbol{S}_{0x}=\begin{bmatrix} 0 \\ -g\cdot h\frac{\partial z}{\partial x} \\ 0 \end{bmatrix}, \quad \boldsymbol{S}_{0y}=\begin{bmatrix} 0 \\ 0 \\ -g\cdot h\frac{\partial z}{\partial y} \end{bmatrix}, \quad \boldsymbol{S}_{fx}=\begin{bmatrix} 0 \\ S_{fx} \\ 0 \end{bmatrix}, \quad \boldsymbol{S}_{fy}=\begin{bmatrix} 0 \\ 0 \\ S_{fy} \end{bmatrix} \tag{3}$$

where $\boldsymbol{U}$ is the vector of conserved variables; $\boldsymbol{F}$ and $\boldsymbol{G}$ are the flux vectors in the x and y directions, respectively; h is the flow depth; u and v are the depth-averaged velocity components in the x and y directions, respectively; S_{0x} and S_{0y} are the bottom slopes; z is the bottom elevation; S_{fx} and S_{fy} are the friction slopes; g is the acceleration due to gravity; t is time. The friction slope is usually expressed using the Manning formula:

$$S_{fx}=\frac{n^2u}{h^{4/3}}\sqrt{u^2+v^2}, \quad S_{fy}=\frac{n^2v}{h^{4/3}}\sqrt{u^2+v^2} \tag{4}$$

where n is the Manning roughness coefficient.

The set (1) can be also rewritten in the quasi-linear form without the source term [5]:

$$\frac{\partial \boldsymbol{U}}{\partial t}+\boldsymbol{A}\frac{\partial \boldsymbol{U}}{\partial x}+\boldsymbol{B}\frac{\partial \boldsymbol{U}}{\partial y}=0 \tag{5}$$

The matrices $\boldsymbol{A}$ and $\boldsymbol{B}$ are the Jacobians of the flux vectors $\boldsymbol{F}$ and $\boldsymbol{G}$, respectively:

$$\boldsymbol{A}=\frac{\partial \boldsymbol{F}}{\partial \boldsymbol{U}}=\begin{bmatrix} 0 & 1 & 0 \\ c^2-u^2 & 2u & 0 \\ -v\cdot u & v & u \end{bmatrix}, \quad \boldsymbol{B}=\frac{\partial \boldsymbol{G}}{\partial \boldsymbol{U}}=\begin{bmatrix} 0 & 0 & 1 \\ -u\cdot v & v & u \\ c^2-v^2 & 0 & 2v \end{bmatrix} \tag{6}$$

where $c=\sqrt{g\cdot h}$ is the wave celerity.

In the set (5), the matrices $\boldsymbol{A}$ and $\boldsymbol{B}$ have three eigenvalues each, given by the relations:

$$\lambda^1=u\cdot n_x+v\cdot n_y-c, \quad \lambda^2=u\cdot n_x+v\cdot n_y, \quad \lambda^3=u\cdot n_x+v\cdot n_y+c \tag{7}$$

and three corresponding eigenvectors:

$$\boldsymbol{r}^1=\begin{bmatrix} 1 \\ u-c\cdot n_x \\ v-c\cdot n_y \end{bmatrix}, \quad \boldsymbol{r}^2=\begin{bmatrix} 0 \\ -n_y \\ n_x \end{bmatrix}, \quad \boldsymbol{r}^3=\begin{bmatrix} 1 \\ u+c\cdot n_x \\ v+c\cdot n_y \end{bmatrix} \tag{8}$$

where n_x and n_y are the components of the unit vector $\boldsymbol{n}=(n_x,n_y)^T$.

The existence of real eigenvalues, λ, means that the shallow water equations are hyperbolic partial differential equations [2, 3]. These equations describe wave propagation with the eigenvalues λ corresponding to the characteristic velocities of the propagating waves.

3. Splitting algorithm for two-dimensional shallow water equations

Two-dimensional shallow water equations can be split according to the coordinate directions, since two-dimensional flow is the sum of flows in the x and y directions [16]. As a result, the solution of the two-dimensional problem is reduced to solving a sequence of one-dimensional problems. The splitting method can be also used with respect to physical processes [3, 16]. According to this method, the shallow water equations are split into two subproblems, thereby describing separately the advection-propagation process and the friction process.

Let us consider the set of equations (1), which can be rewritten in the form:

$$\frac{\partial \boldsymbol{U}}{\partial t} = \boldsymbol{Y} \tag{9}$$

where the vector $\boldsymbol{Y}$ represents all the terms of the set (1), except for the time derivatives. The solution of Equations (9) is obtained by integrating over time, in the range $[t,t+\Delta t]$:

$$\boldsymbol{U}^{n+1} = \boldsymbol{U}^{n} + \int_{t}^{t+\Delta t} \boldsymbol{Y}\, dt \tag{10}$$

where $\boldsymbol{U}^n$ and $\boldsymbol{U}^{n+1}$ are the vectors at time t and $t+\Delta t$, respectively. Taking into account the dimensional and physical splitting, the vector $\boldsymbol{Y}$ can be expressed as a sum of three vectors:

$$\boldsymbol{Y} = \boldsymbol{Y}^{(1)} + \boldsymbol{Y}^{(2)} + \boldsymbol{Y}^{(3)} \tag{11}$$

where:

$$\boldsymbol{Y}^{(1)} = -\frac{\partial \boldsymbol{F}}{\partial x} + \boldsymbol{S}_{0x}, \quad \boldsymbol{Y}^{(2)} = -\frac{\partial \boldsymbol{G}}{\partial y} + \boldsymbol{S}_{0y}, \quad \boldsymbol{Y}^{(3)} = \boldsymbol{S}_{fx} + \boldsymbol{S}_{fy} \tag{12}$$

The vector $\boldsymbol{Y}^{(3)}$ contains only the friction term, whereas the vectors $\boldsymbol{Y}^{(1)}$ and $\boldsymbol{Y}^{(2)}$ contain all the remaining terms, which correspond to the x and y direction, respectively. Substituting (11) and (12) into (9) we obtain a set of the following form:

$$\frac{\partial \boldsymbol{U}}{\partial t} = \boldsymbol{Y}^{(1)} + \boldsymbol{Y}^{(2)} + \boldsymbol{Y}^{(3)} \tag{13}$$

Thus, the SWEs are decomposed into three separate sets and the solution algorithm proceeds in three stages for each time step Δt. In the first stage, we solve a set of one-dimensional equations in the x direction:

$$\frac{\partial \boldsymbol{U}^{(1)}}{\partial t} = \boldsymbol{Y}^{(1)} \tag{14}$$

with the initial condition $\boldsymbol{U}^{(1)t} = \boldsymbol{U}^{t}$. Subsequently, the solution $\boldsymbol{U}^{(1)t+\Delta t}$ of Equation (14) is taken in the second stage as the initial condition $\boldsymbol{U}^{(2)t} = \boldsymbol{U}^{(1)t+\Delta t}$ for the set of one-dimensional equations in the y direction:

$$\frac{\partial \boldsymbol{U}^{(2)}}{\partial t} = \boldsymbol{Y}^{(2)} \tag{15}$$

Then, in the third stage, we solve the equation containing only the friction term:

$$\frac{\partial \boldsymbol{U}^{(3)}}{\partial t} = \boldsymbol{Y}^{(3)} \tag{16}$$

with the initial condition $\boldsymbol{U}^{(3)t} = \boldsymbol{U}^{(2)t+\Delta t}$. The integration of Equation (16) finally gives the solution $\boldsymbol{U}^{t+\Delta t} = \boldsymbol{U}^{(3)t+\Delta t}$ at time $t = t + \Delta t$.

The use of the dimensional splitting leads to a more effective algorithm compared to the standard method of approximation. Additionally, the splitting with regard to the physical processes (friction) ensures proper incorporation of the friction source term into the algorithm of finite volume methods.

The accuracy and stability of the presented splitting algorithm depend on the method used for the solution of each subproblem described by Equations (14)–(16). During the decomposition of the non-linear equations, a splitting error is introduced into the solution. In this case, the splitting error depends on the time step Δt and it is therefore possible to minimize this error by reducing the time step Δt [5].

4. Finite volume method

The finite volume method is based on the integral form of the governing equations written for an elementary finite volume (cell). Let us consider a single finite volume in a two-dimensional rectangular grid (Figure 1). The area of a cell is bounded by its edges, where $\Delta x = x_{i+\frac{1}{2},j} - x_{i-\frac{1}{2},j}$ and $\Delta y = y_{i,j+\frac{1}{2}} - y_{i,j-\frac{1}{2}}$.

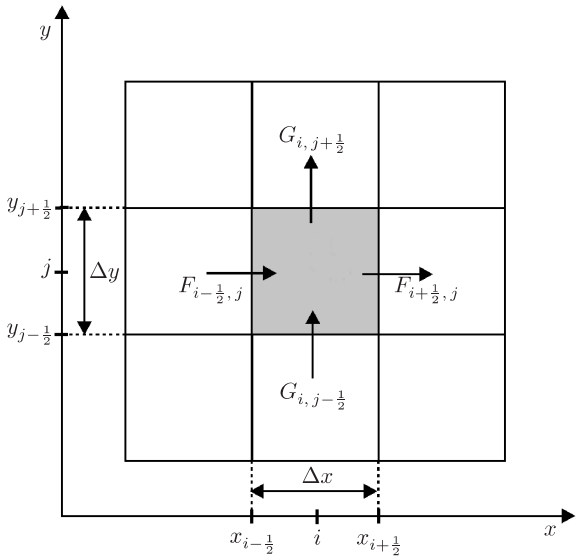

Figure 1. Finite volume cell in two dimensions, the vector $\boldsymbol{U}_{i,j}$ represents a cell average, the vectors $\boldsymbol{F}_{i-\frac{1}{2},j}$, $\boldsymbol{F}_{i+\frac{1}{2},j}$ and $\boldsymbol{G}_{i,j-\frac{1}{2}}$, $\boldsymbol{G}_{i,j+\frac{1}{2}}$ represent the numerical fluxes at the cell edges in the x and y directions, respectively

Taking a constant length of the cell edges ($\Delta x = \Delta y = \text{const}$) and integrating the system (1) without the source term over the cell volume and over time, a fully discrete form of the two-dimensional shallow water equations is obtained:

$$\boldsymbol{U}_{i,j}^{t+\Delta t} = \boldsymbol{U}_{i,j}^{t} - \frac{\Delta t}{\Delta x}\left[\boldsymbol{F}_{i-\frac{1}{2},j}^{t} - \boldsymbol{F}_{i+\frac{1}{2},j}^{t}\right] - \frac{\Delta t}{\Delta y}\left[\boldsymbol{G}_{i,j-\frac{1}{2}}^{t} - \boldsymbol{G}_{i,j+\frac{1}{2}}^{t}\right] \tag{17}$$

The vector $\boldsymbol{U}_{i,j}$ approximates a cell average over the grid cell (i,j) at time t:

$$\boldsymbol{U}_{i,j} \approx \frac{1}{\Delta x \cdot \Delta y} \int_{y_{i-\frac{1}{2}}}^{y_{i+\frac{1}{2}}} \int_{x_{i-\frac{1}{2}}}^{x_{i+\frac{1}{2}}} \boldsymbol{U}(x,y,t)\,dx\,dy \tag{18}$$

and the vectors $\boldsymbol{F}_{i-\frac{1}{2},j}$ and $\boldsymbol{G}_{i,j-\frac{1}{2}}$ are the numerical fluxes through the edges of the cell in the x and y directions, respectively. The value of the flux in the corresponding direction (x or y) is based on the values of $\boldsymbol{U}^n$ in the adjacent cells.

Let us consider a rectangular spatial grid with M columns and N rows. According to the splitting algorithm, in the first step the set of one-dimensional equations (14) in the x direction can be solved for each row of cells with fixed j ($j = 1,2,\ldots,N$). As a result, the following equation is obtained:

$$\boldsymbol{U}_{i,j}^{(1)t+\Delta t} = \boldsymbol{U}_{i,j}^{(1)t} - \frac{\Delta t}{\Delta x}\left[\boldsymbol{F}_{i-\frac{1}{2},j}^{(1)t} - F_{i+\frac{1}{2},j}^{(1)t}\right] \text{ with } \boldsymbol{U}^{(1)t} = \boldsymbol{U}^{t} \tag{19}$$

Similarly, during the second stage, the one-dimensional set (15) in the y direction for columns of cells with i fixed ($i = 1,2,\ldots,M$) is computed as follows:

$$\boldsymbol{U}_{i,j}^{(2)t+\Delta t} = \boldsymbol{U}_{i,j}^{(2)t} - \frac{\Delta t}{\Delta y}\left[\boldsymbol{G}_{i,j-\frac{1}{2}}^{(2)t} - \boldsymbol{G}_{i,j+\frac{1}{2}}^{(2)t}\right] \text{ with } \boldsymbol{U}^{(2)t} = \boldsymbol{U}^{(1)t+\Delta t} \tag{20}$$

where $\boldsymbol{F}_{i-\frac{1}{2},j}$ and $\boldsymbol{G}_{i,j-\frac{1}{2}}$ are the numerical fluxes at the cell edge for one-dimensional problems in the x and y directions, respectively.

4.1. Determination of the numerical flux

The properties (stability and accuracy) of a numerical scheme depend on how the numerical flux at the cell edges is determined. In the finite volume method, the Roe algorithm [17], based on the approximate solution of the Riemann problem is the most popular algorithm for the computation of the numerical flux. The standard solution of the one-dimensional Riemann problem between states $\boldsymbol{U}_i$ and $\boldsymbol{U}_{i-1}$ in cells i and $i-1$ can be determined by decomposing the increment of the dependent variables $\Delta\boldsymbol{U} = \boldsymbol{U}_i - \boldsymbol{U}_{i-1}$ into a linear combination of eigenvectors $\boldsymbol{r}^k$ of the matrix $\boldsymbol{A}$ [14]:

$$\Delta\boldsymbol{U} = \boldsymbol{U}_i - \boldsymbol{U}_{i-1} = \sum_{k=1}^{m} \alpha_{i-\frac{1}{2}}^{k} \boldsymbol{r}_{i-\frac{1}{2}}^{k} \tag{21}$$

In this case, the solution of the Riemann problem consists of m waves propagating at a speed associated with eigenvalue λ^k. Each wave is proportional to the eigenvector $\boldsymbol{r}^k$ (where α^k is the proportionality coefficient). An alternative

approach was presented by Bale *et al.* [15], where instead of decomposing $\Delta \boldsymbol{U}$ in terms of dependent variables $\boldsymbol{U}$, the splitting into eigenvectors $\boldsymbol{r}^k$ was performed for the increment of the flux $\Delta \boldsymbol{F}(\boldsymbol{U})$ as follows:

$$\Delta \boldsymbol{F}(\boldsymbol{U}) = \boldsymbol{F}_i(\boldsymbol{U}_i) - \boldsymbol{F}_{i-1}(\boldsymbol{U}_{i-1}) = \sum_{k=1}^{m} \beta_{i-\frac{1}{2}}^k \boldsymbol{r}_{i-\frac{1}{2}}^k = \sum_{k=1}^{m} \boldsymbol{Z}_{i-\frac{1}{2}}^k \tag{22}$$

where vector $\boldsymbol{Z}^k$ is termed an f-wave and carries the increment in $\boldsymbol{F}$, across the wave propagating with a celerity λ^k. In the case of the two-dimensional shallow water equations, a set of three waves ($k = 1,2,3$) and the coefficient $\beta_{1-\frac{1}{2}}$ are determined by the following formula:

$$\beta_{i-\frac{1}{2}} = \boldsymbol{R}_{i-\frac{1}{2}}^{-1} \left(\boldsymbol{F}_i(\boldsymbol{U}_i) - \boldsymbol{F}_{i-1}(\boldsymbol{U}_{i-1}) \right) \tag{23}$$

where $\boldsymbol{R}_{1-\frac{1}{2}}$ is the matrix of eigenvectors $\boldsymbol{r}$.

The application of the Roe method to the two-dimensional shallow water equations leads to an average value of the flow parameters at the cell edge between the states $\boldsymbol{U}_i$ and $\boldsymbol{U}_{i-1}$. These parameters are determined as follows [4]:

$$\bar{h}_{i-\frac{1}{2}} = \frac{h_i + h_{i-1}}{2} \tag{24}$$

$$\bar{u}_{i-\frac{1}{2}} = \frac{u_i\sqrt{h_i} + u_{i-1}\sqrt{h_{i-1}}}{\sqrt{h_i} + \sqrt{h_{i-1}}} \tag{25}$$

$$\bar{v}_{i-\frac{1}{2}} = \frac{v_i\sqrt{h_i} + v_{i-1}\sqrt{h_{i-1}}}{\sqrt{h_i} + \sqrt{h_{i-1}}} \tag{26}$$

where the water depth $\bar{h}_{i-\frac{1}{2}}$ and the velocities $\bar{u}_{i-\frac{1}{2}}$, $\bar{v}_{i-\frac{1}{2}}$ are the Roe averages used for the computation of average values of the coefficient $\bar{\beta}$ (Equation (23)) and the f-waves. $\boldsymbol{Z}$ is calculated according to Equation (22).

Using Equation (22) in Equations (20) according to the Roe method yields the wave-propagation algorithm for the x direction:

$$\boldsymbol{U}_{i,j}^{(1)t+\Delta t} = \boldsymbol{U}_{i,j}^{(1)t} - \frac{\Delta t}{\Delta x} \left[\sum_{k=1,\lambda<0}^{m} \boldsymbol{Z}_{i+\frac{1}{2},j}^k + \sum_{k=1,\lambda>0}^{m} \boldsymbol{Z}_{i-\frac{1}{2},j}^k \right] \tag{27}$$

A similar procedure is used for the y direction, leading to:

$$\boldsymbol{U}_{i,j}^{(2)t+\Delta t} = \boldsymbol{U}_{i,j}^{(2)t} - \frac{\Delta t}{\Delta x} \left[\sum_{k=1,\lambda<0}^{m} \boldsymbol{Z}_{i,j+\frac{1}{2}}^k + \sum_{k=1,\lambda>0}^{m} \boldsymbol{Z}_{i,j-\frac{1}{2}}^k \right] \tag{28}$$

According to the presented algorithm, a one-dimensional Riemann problem is solved for each stage in the corresponding direction. Moreover, from Equation (27), it follows that the cell average $\boldsymbol{U}_{i,j}$ in the x direction is affected by all the left-going f-waves from $x_{i+\frac{1}{2},j}$ and all right-going f-waves from $x_{i-\frac{1}{2},j}$. In a similar way, the average $\boldsymbol{U}_{i,j}$ is influenced by all waves in the y direction.

The presented scheme belongs to the class of Godunov-type schemes and is only first-order accurate in space as well as in time. In order to improve the

accuracy, the numerical flux is suitably modified by introducing an additional correction term. The form of this term is based on the well-known Lax-Wendroff scheme [5, 18]. Thus, high-resolution corrections and dimensional splitting applied to the wave-propagation algorithm produce a two-stage numerical scheme in the x direction:

$$\boldsymbol{U}_{i,j}^{(1)t+\Delta t}=\boldsymbol{U}_{i,j}^{(1)t}-\frac{\Delta t}{\Delta x}\left[\sum_{k=1,\lambda<0}^{m}\boldsymbol{Z}_{i+\frac{1}{2},j}^{k}+\sum_{k=1,\lambda>0}^{m}\boldsymbol{Z}_{i-\frac{1}{2},j}^{k}\right]-\frac{\Delta t}{\Delta x}\left[\boldsymbol{F}_{i+\frac{1}{2},j}^{C}-\boldsymbol{F}_{i-\frac{1}{2},j}^{C}\right] \quad (29)$$

and in the y direction:

$$\boldsymbol{U}_{i,j}^{(2)t+\Delta t}=\boldsymbol{U}_{i,j}^{(2)t}-\frac{\Delta t}{\Delta x}\left[\sum_{k=1,\lambda<0}^{m}\boldsymbol{Z}_{i,j+\frac{1}{2}}^{k}+\sum_{k=1,\lambda>0}^{m}\boldsymbol{Z}_{i,j-\frac{1}{2}}^{k}\right]-\frac{\Delta t}{\Delta y}\left[\boldsymbol{G}_{i,j+\frac{1}{2}}^{C}-\boldsymbol{G}_{i,j-\frac{1}{2}}^{C}\right] \quad (30)$$

where the correction fluxes $\boldsymbol{F}_{i-\frac{1}{2},j}^{C}$ and $\boldsymbol{G}_{i,j-\frac{1}{2}}^{C}$ are computed from:

$$\boldsymbol{F}_{i-\frac{1}{2},j}^{C}=\frac{1}{2}\sum_{k=1}^{m}\left(\boldsymbol{I}-\frac{\Delta t}{\Delta x}\operatorname{sgn}(\lambda_{i-\frac{1}{2},j}^{k})\right)\boldsymbol{Z}_{i-\frac{1}{2},j}^{k}\phi_{i-\frac{1}{2},j} \quad (31)$$

$$\boldsymbol{G}_{i,j-\frac{1}{2}}^{C}=\frac{1}{2}\sum_{k=1}^{m}\left(\boldsymbol{I}-\frac{\Delta t}{\Delta x}\operatorname{sgn}(\lambda_{i,j-\frac{1}{2}}^{k})\right)\boldsymbol{Z}_{i,j-\frac{1}{2}}^{k}\phi_{i,j-\frac{1}{2}} \quad (32)$$

The function ϕ is the flux-limiter function assuming values from [0;1]. This function changes the value of the correction flux according to the numerical solution. For $\phi=1$, the scheme is second-order accurate for a smooth solution and is consistent with the Lax-Wendroff scheme. For a solution with a discontinuity or steep gradient, a lower-order scheme must be applied in order to damp the non-physical oscillations. The attenuation of these oscillations is caused by numerical diffusion in the solution. Maximum numerical diffusion is obtained for $\phi=0$, and then the resulting scheme is upwind with a first-order accuracy. In practical cases, numerical diffusion is introduced in a controlled way, by a proper choice of the flux-limiter function ϕ, which minimizes numerical diffusion for a smooth solution or eliminates unphysical oscillations for a discontinuity solution. A review of flux-limiter functions can be found in Toro [4] and Leveque [5]. In this study, the Van Leer function is assumed, which is given by the formula:

$$\phi(\theta)=\frac{\theta+|\theta|}{1+|\theta|} \quad (33)$$

where θ is the smoothness of the solution at $x_{i-\frac{1}{2}}$. The value of the smoothness is obtained by comparing the corresponding waves $\boldsymbol{W}^{k}=\boldsymbol{Z}^{k}/\lambda^{k}$ in neighboring cells, as follows:

$$\left|\theta_{i-\frac{1}{2}}\right|=\frac{\left\|W_{I-\frac{1}{2}}^{k}\right\|}{\left\|W_{i-\frac{1}{2}}^{k}\right\|},\quad I=\begin{cases}i-1 & \text{for } \lambda^{k}>0\\ i+1 & \text{for } \lambda^{k}<0\end{cases} \quad (34)$$

The presented algorithm is second-order accurate for a smooth solution and is a variant of the Lax-Wendroff method. This algorithm gives a stable solution, if the following condition is satisfied [14]:

$$\mathrm{Cr} = \max\left(\lambda_x \frac{\Delta t}{\Delta x}, \lambda_y \frac{\Delta t}{\Delta y}\right) \tag{35}$$

where Cr is the Courant number, and λ_x and λ_y are the maximum wave speeds in the x and y direction, respectively.

The solution of the SWEs for the Riemann problem consists of both shock and rarefaction waves. Unfortunately, the Roe method leads to an approximate solution, which correctly reproduces only the shock wave, while the rarefaction wave is not taken into account. This leads to the violation of the entropy condition [5] and, as a result, unphysical effects are observed in the numerical solution. In this case, a modification of the approximate Riemann solver is required in order to obtain the correct solution satisfying the entropy condition. In this paper, the method proposed by Harten and Hyman was applied [5]. This approach is based on a modification of the eigenvalues. If a transonic rarefaction wave appears in the numerical solution, *i.e.*:

$$\lambda^k(\boldsymbol{U}_{i-1}) < 0 < \lambda^k(\boldsymbol{U}_i) \quad (k = 1,2,3) \tag{36}$$

is satisfied, then the eigenvalues are corrected as follows:

$$(\bar{\lambda}^k)^- = \frac{\lambda_i^k - \bar{\lambda}^k}{\lambda_i^k - \lambda_{i-1}^k}\lambda_{i-1}^k, \quad (\bar{\lambda}^k)^+ = \left(1 - \frac{\lambda_i^k - \bar{\lambda}^k}{\lambda_i^k - \lambda_{i-1}^k}\right)\lambda_i^k \tag{37}$$

where $\bar{\lambda}^k$ are the Roe average eigenvalues.

4.2. Approximation of source terms

Improper treatment of the source terms in the algorithm of the finite volume method can cause significant complications, leading to inaccurate solutions. This problem is particularly evident in the case of the bottom source term, which must be incorporated into the flow occurring over a bottom with a variable slope [19, 20]. Another difficulty arises from the improper treatment of the friction source term during the simulation of supercritical flow with a very small depth and high speeds. In such a case, the inaccurate approximation of the bottom and friction source terms can cause non-physical oscillations, which may then lead to a breakdown of the calculations.

It is possible to obtain a suitable approximation of the bottom source term by using the flux-based wave decomposition expressed by Equation (22) [15]. To this effect, the source term $\boldsymbol{S}_0$ is approximated at the cell edges and then incorporated into the flux differences $\boldsymbol{F}(\boldsymbol{U})$ in the following way:

$$\boldsymbol{F}_{i,j}(\boldsymbol{U}_{i,j}) - \boldsymbol{F}_{i-1,j}(\boldsymbol{U}_{i-1,j}) - \Delta x \cdot \boldsymbol{S}_{0xi-\frac{1}{2},j} = \sum_{k=1}^{m} \beta_{i-\frac{1}{2},j}^k \boldsymbol{r}_{i-\frac{1}{2},j}^k = \sum_{k=1}^{m} \boldsymbol{Z}_{i-\frac{1}{2},j}^k \tag{38}$$

where the source term $\boldsymbol{S}_{0xi-\frac{1}{2},j}$ in the x direction is approximated at the cell edge $x_{1-\frac{1}{2}}$, as follows:

$$\boldsymbol{S}_{0xi-\frac{1}{2},j} = \begin{bmatrix} 0 \\ -g\frac{(h_{i-1,j}+h_{i,j})}{2}\frac{(z_{i,j}-z_{i-1,j})}{\Delta x} \\ 0 \end{bmatrix} \tag{39}$$

In this case, the coefficient β is computed using the following formula:

$$\beta_{i-\frac{1}{2}} = \boldsymbol{R}^{-1}_{i-\frac{1}{2}} \left(\boldsymbol{F}_i(\boldsymbol{U}_i) - \boldsymbol{F}_{i-1}(\boldsymbol{U}_{i-1}) - \Delta x \boldsymbol{S}_{0xi-\frac{1}{2},j} \right) \tag{40}$$

In a similar way, the discretization of the source term in the y direction gives the relation:

$$\boldsymbol{S}_{0yi,j-\frac{1}{2}} = \begin{bmatrix} 0 \\ 0 \\ -g\frac{(h_{i,j-1}+h_{i,j})}{2}\frac{(z_{i,j}-z_{i,j-1})}{\Delta y} \end{bmatrix} \tag{41}$$

In order to overcome the problem of approximation of the friction source term $\boldsymbol{S}_f$, the splitting method with respect to physical processes was applied. As a result, in the third stage of splitting, we obtained Equation (16), containing only the friction term:

$$\frac{\partial \boldsymbol{U}^{(3)}}{\partial t} = \boldsymbol{Y}^{(3)} \tag{42}$$

The solution of Equation (42) corresponds to the integration in time of two simplified dynamic equations:

$$\frac{\partial(u \cdot h)}{\partial t} = S_{fx}, \quad \frac{\partial(v \cdot h)}{\partial t} = S_{fy} \tag{43}$$

Application of the implicit method for Equations (43) gives a set of two nonlinear algebraic equations, which can be solved by means of the Newton method.

5. Numerical tests

5.1. One-dimensional dam-break problem

In this numerical test, the one-dimensional dam-break problem is considered for a rectangular frictionless channel 500 m long and 1 m wide, with a bottom slope equal to 0. The dam is located at $x = 250\,\mathrm{m}$ and divides the domain into two areas with different depths, h_L and h_R. The initial condition at time $t = 0$ corresponds to the water being at rest with the following depths:

$$h(x,0) = \begin{cases} h_L = 10\,\mathrm{m} & \text{for } x \le 250\,\mathrm{m} \\ h_R = 2\,\mathrm{m} & \text{for } x \ge 250\,\mathrm{m} \end{cases}$$

At the upstream end of the boundary, $x = 0$, the velocity $u_L(t) = 0$ is imposed and at the downstream boundary, $x = 500\,\mathrm{m}$, a constant water depth $h_R(t) = 2\,\mathrm{m}$ is imposed. It was assumed that at the initial time, the dam is instantaneously broken, which leads to a discontinuity. Consequently, a shock wave propagates downstream and, at the same time, a rarefaction wave propagates upstream (Figure 2, panel (a)). The computations were carried out for $\Delta x =$

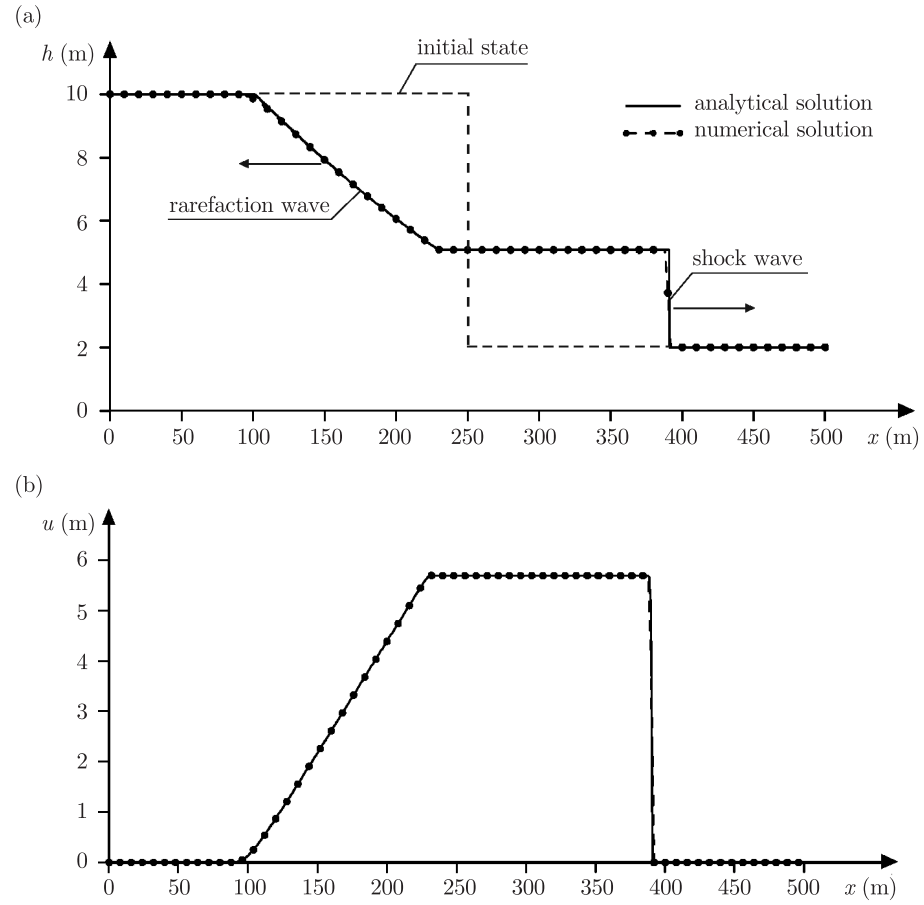

Figure 2. Comparison of analytical and numerical solution at time $t = 15\,\mathrm{s}$ for: (a) depth and (b) velocity

0.5 m and $\Delta t = 0.015\,\mathrm{s}$. For the assumed initial-boundary conditions, the one-dimensional shallow water equations have an analytical solution [21, 22]. The results of numerical simulations and the analytical solution for depth h and velocity u are presented in Figure 2, which shows good agreement between the corresponding solutions.

5.2. Two-dimensional dam-break problem

This numerical test demonstrates a two-dimensional dam-break study using a homogeneous system of the SWEs (frictionless and flat-bottom). The spatial domain, 200 m long and 200 m wide, was covered by a rectangular grid with $\Delta x = \Delta y = 5\,\mathrm{m}$. The dam breach of the length $D = 75\,\mathrm{m}$ is situated at $x = 100\,\mathrm{m}$ (Figure 3). At the initial time $t = 0$, the water body is at rest with water depths $h_L = 10$ m in the upstream and $h_R = 5\,\mathrm{m}$ in the downstream part of the reservoir, respectively. Moreover, at $x = 200\,\mathrm{m}$, an open boundary is imposed in the form of a constant water depth $h(x = 200, y, t \geq 0) = h_R = 5\,\mathrm{m}$. Closed boundary conditions

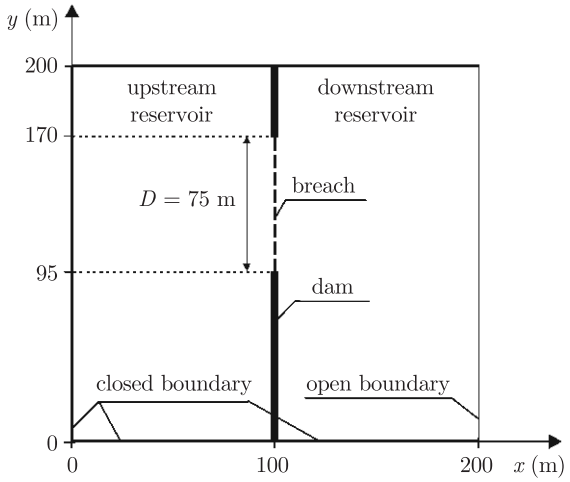

Figure 3. Domain of the two-dimensional dam-break problem

with a normal unit discharge $q_n = 0$ are also imposed. The calculations were carried out with a time step of $\Delta t = 0.1\,\mathrm{s}$.

Figure 4 presents a numerical simulation, after a dam-break at time $t = 7.2\,\mathrm{s}$, in the form of the water surface. Additionally, Figure 5 shows the velocity field for the same time. Figure 4 demonstrates that after the dam failure, a shock wave propagates downstream through a breach and a rarefaction wave propagates in the upstream part of the reservoir. Unfortunately, there is no analytical solution for the two-dimensional problem. The obtained numerical results show that the two-dimensional flow is adequately simulated and these results are in good agreement with the results presented in [9, 12, 23].

5.3. Two-dimensional dike-break problem

This numerical test simulation was carried out for a dike-break problem. In this case, the upstream reservoir is replaced by an open channel, where steady flow conditions are assumed. The spatial domain consists of a rectangular channel of the length $L = 500\,\mathrm{m}$, width $B = 50\,\mathrm{m}$, with a bottom slope $s = 0.0005$ and a flood plain of the dimensions $200 \times 500\,\mathrm{m}$ with a zero bottom slope (Figure 6). The channel was separated from the floodplain by a dike of the thickness $d = 5\,\mathrm{m}$. In the channel, as well as in the flood plain, a constant Manning roughness coefficient $n = 0.025\,\mathrm{m}^{-1/3}\mathrm{s}$ was assumed.

At the initial time, steady flow was assumed in the channel, with a depth of $h_p = 5\,\mathrm{m}$ and unit discharge $q_y = 13\,\mathrm{m}^2/\mathrm{s}$ in the y direction and a zero unit discharge in the x direction ($q_x = 0$). In the flood plain, water is at rest ($q_x = q_y = 0$) with a constant depth $h = 0.0001\,\mathrm{m}$, which corresponds to the so-called dry-state conditions. At the upstream boundary of the channel, a constant unit discharge equal to the initial inflow was imposed, whereas at the downstream end, the depth remains equal to the initial state until the dike-break. It is assumed that in an infinitely short time, the dike is broken at a length of 40 m. After

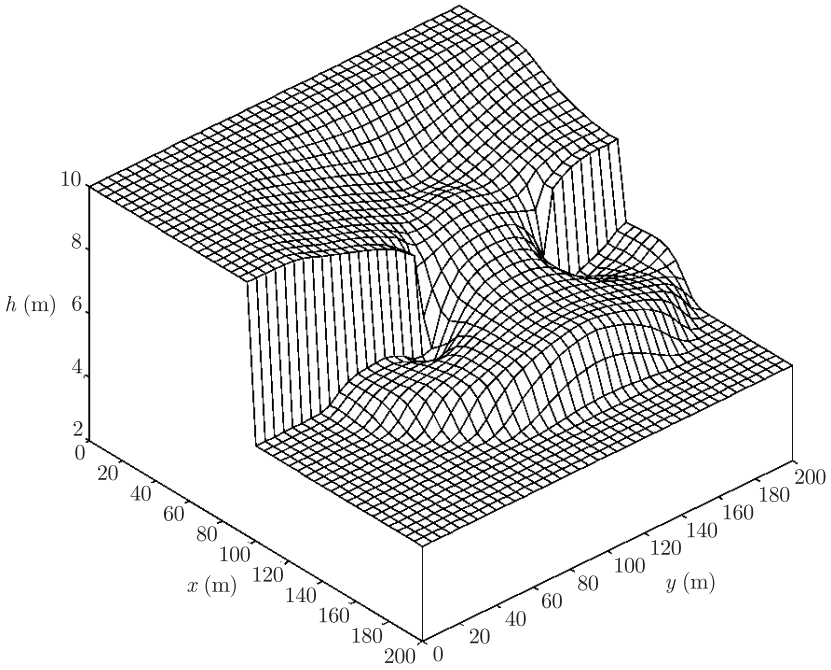

Figure 4. Water surface at $t = 7.2$ s after the dam-break

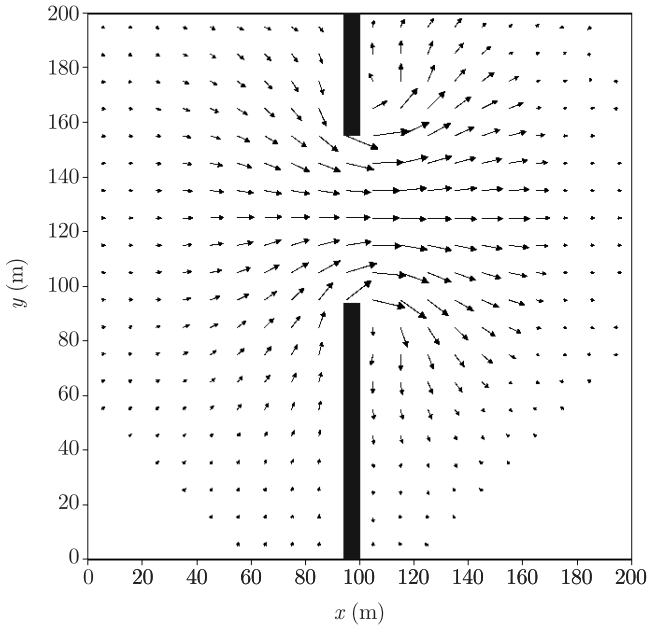

Figure 5. Velocity field at $t = 7.2$ s after the dam-break

this time, the disturbances in the form of rarefaction waves propagate in the channel. Moreover, a certain fraction of the water volume outflows through the breach during the simulation. Thus, at the downstream boundary of the channel,

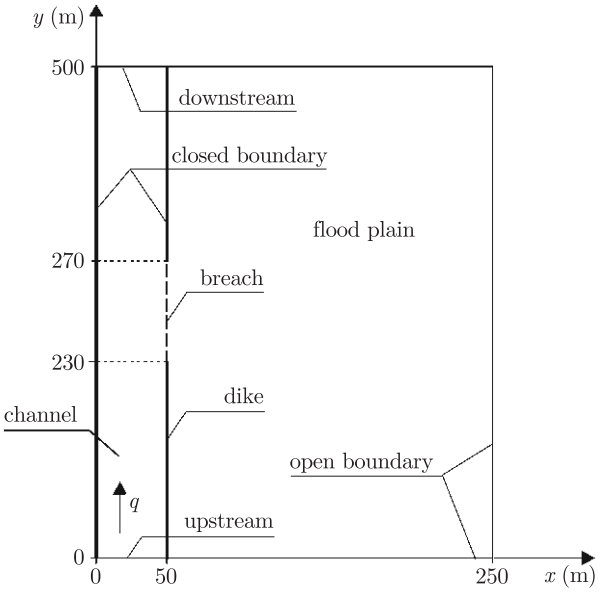

Figure 6. Domain for the two-dimensional dike-break problem

depth and discharge are usually unknown functions, which vary in time. In order to determine the downstream boundary condition, a zero gradient of depth was applied. In such a case, it is also possible to apply the relationship in the form of the Riemann invariant [1, 5, 10]. However, these simplifications may introduce a significant error into the numerical solution.

At the open boundaries of the flood plain, a constant water depth $h_R(t) = 0.0001\,\mathrm{m}$ was imposed before the shock wave reached the open boundary. Subsequently, no condition was implemented due to supercritical flow. At the closed boundary, the unit discharge in the normal direction was set to zero ($q_n = 0$). The spatial domain was covered by a square grid with $\Delta x = \Delta y = 5\,\mathrm{m}$ and the calculations were carried out with a time step of $\Delta t = 0.1\,\mathrm{s}$ for the simulation time $t = 40\,\mathrm{s}$. Additionally, the same domain was used to compute the dam-break induced flow and to compare it with the results obtained during the dike-break simulation. For this purpose, the discharge in the channel was set to zero. The remaining initial-boundary conditions were the same as for the dike-break test. Figure 7 presents the results of numerical solutions in the form of the water surface. Here, (*cf.* Figure 7, panel (a)) the propagating rarefaction waves in the channel are asymmetrical, unlike in the case with the initial discharge in channel set to zero (Figure 7, panel (b)).

An asymmetric wave propagation for the dike-break simulation results from the inflow through the upper edge of the channel. This effect is clearly visible in Figure 8, where the results are presented in the form of depth isolines. For the dam-break simulation, zero discharge in the upstream part of the reservoir was assumed. Consequently, after a certain time, the upper reservoir is completely

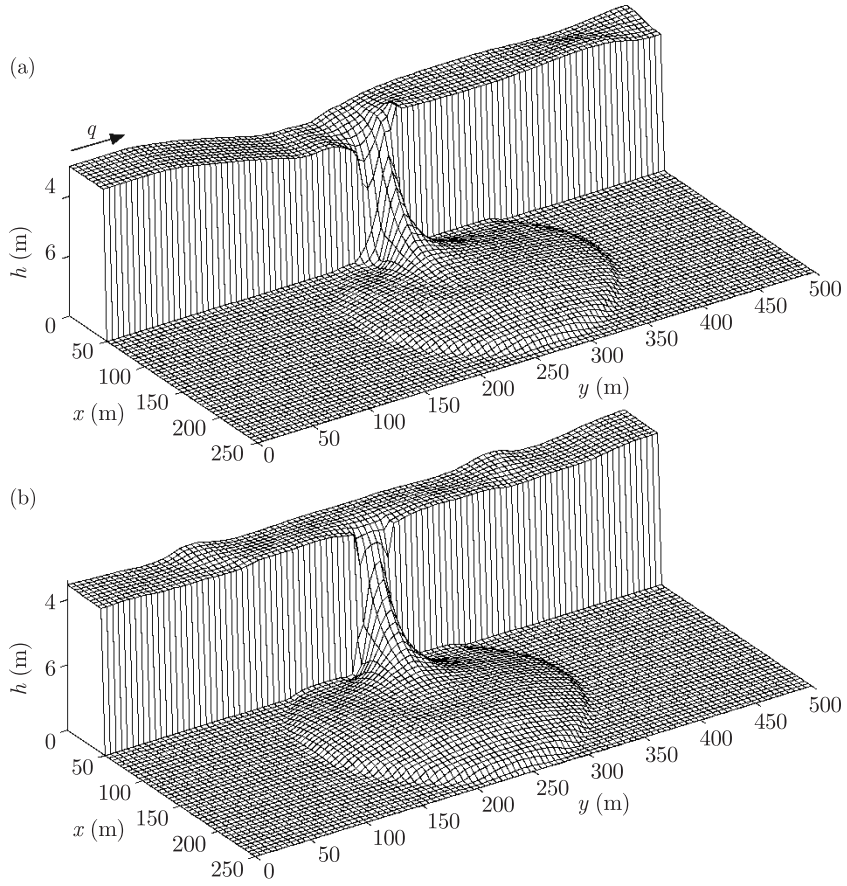

Figure 7. Water surface at $t = 40\,\mathrm{s}$ after the dike-break: (a) with the initial flow in the channel $q_p = 13\,\mathrm{m}^2/\mathrm{s}$; (b) without the initial flow in the channel $q_p = 0\,\mathrm{m}$

emptied due to water outflowing through the breach. This situation does not take place in the case of the dike-break where the imposed flow at the upper end of the channel causes a continuous flow into the channel as well as into the flood plain during the entire simulation period.

5.4. Comparison of numerical results and physical experiments

5.4.1. Two-dimensional dike-break problem

The physical experiment was conducted by Aureli and Mignosa [11] in a hydraulic laboratory at the University of Parma, Italy. The data were obtained during tests in a rectangular channel of the length $L = 5.55\,\mathrm{m}$, width $B = 0.3\,\mathrm{m}$, and with a constant bed slope $s = 0.001$. The channel was connected to the flood plain through a movable wall of the width $b = 0.28\,\mathrm{m}$. The geometry of the hydraulic model and the deployment of the gauges measuring the depths are shown in Figure 9. For the channel and the flood plain, a constant value of $n = 0.01\,\mathrm{m}^{-1/3}\mathrm{s}$ was assumed for the Manning roughness coefficient. At the initial

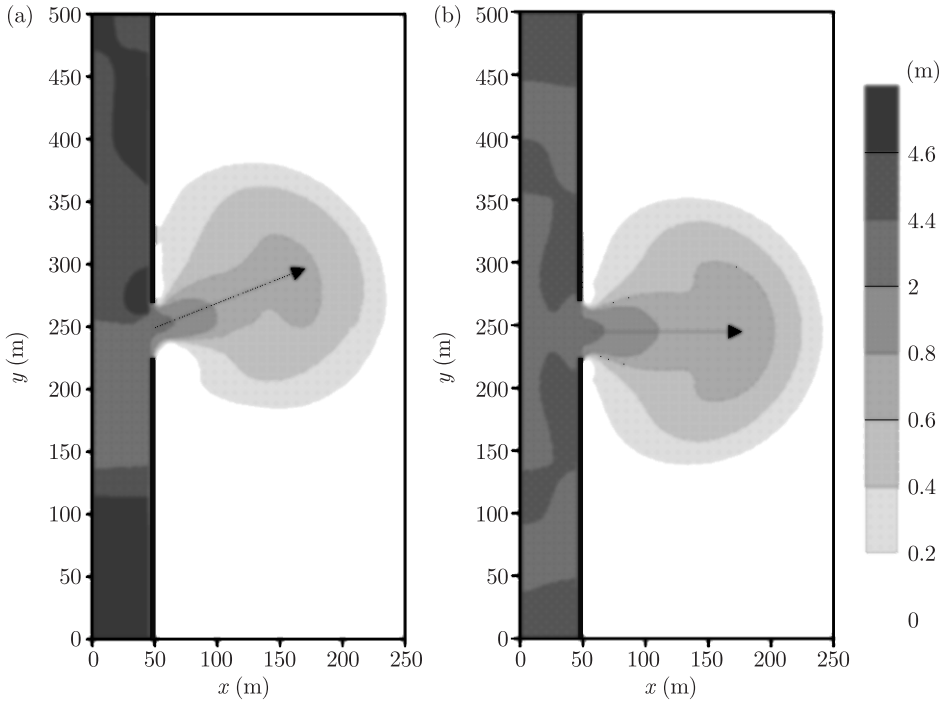

Figure 8. Depths at time $t = 40\,\mathrm{s}$ after the dike-break: (a) with the initial flow in the channel, $q_p = 13\,\mathrm{m}^2/\mathrm{s}$; (b) without the initial flow, $q_p = 0$

time, steady flow in the channel was induced with a discharge $Q_p = 0.01\,\mathrm{m}^3/\mathrm{s}$ and depth $h_p = 0.0794\,\mathrm{m}$. At the same time, dry state was maintained in the flood plain.

The laboratory experiment was reproduced using a presented numerical model. It was assumed that in an infinitely short time, the dike was broken over a length of $b = 0.28\,\mathrm{m}$. The calculations were carried out for a rectangular mesh $\Delta x = \Delta y = 0.02\,\mathrm{m}$ with a time step of $\Delta t = 0.002\,\mathrm{s}$. Figure 10 shows a comparison between the numerical calculations and the results of physical experiments for selected points. The results in the form of time series for the specified depths show good agreement with numerical solutions at points P1 and P2. However, such agreement was not obtained for points P3 and P4. These discrepancies can be caused by the complex structure of the flow and the significant curvatures of the surface near the breach. This serves to illustrate that real, three-dimensional flow is difficult to simulate by means of a two-dimensional depth-averaged model. Moreover, the authors of the laboratory experiment [11] suggested that the reflections at the boundaries of small disturbances are very hard to measure in real fluids.

5.4.2. Two-dimensional dam-break problem with an obstacle

The second experiment involved a dam-break induced flow around an obstacle representing a building. The physical experiment was conducted by

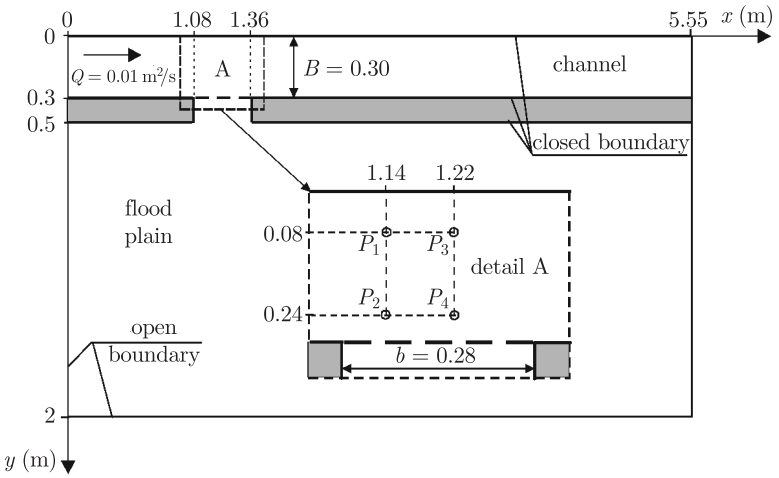

Figure 9. Geometry of the hydraulic model (Aureli and Mignosa [11])

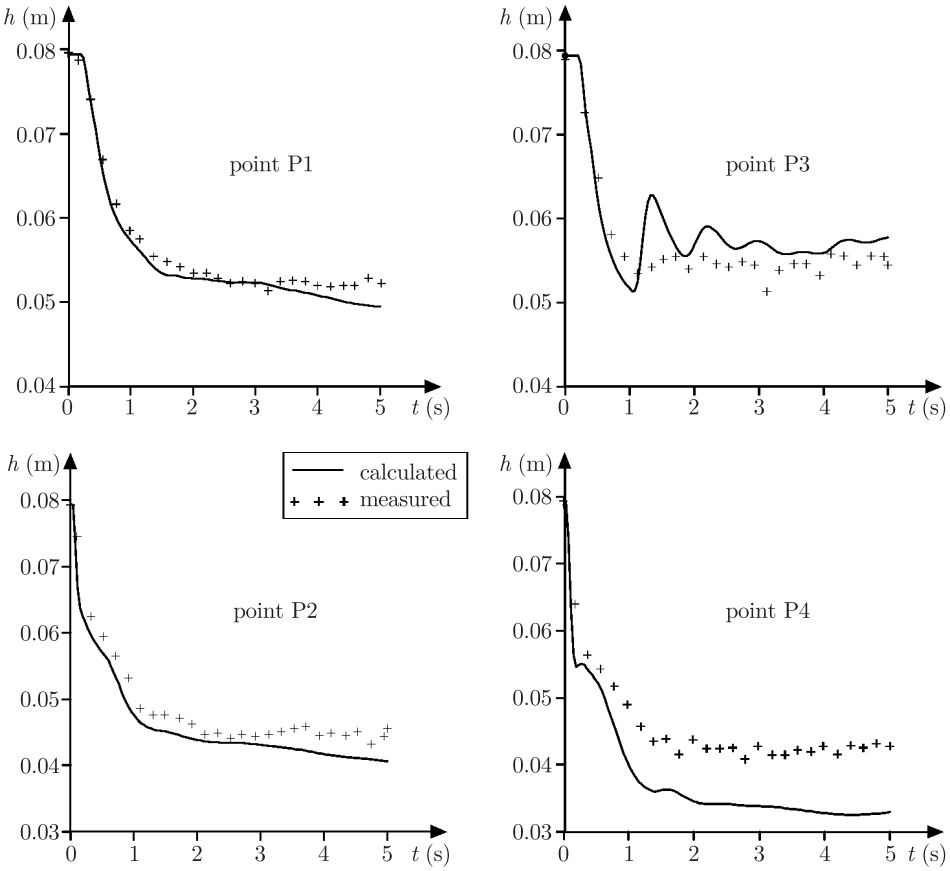

Figure 10. Comparison of measured and calculated depths at point P1, P2, P3 and P4

Szydłowski [24] in a hydraulic laboratory at the Gdansk University of Technology, Poland. The geometry of the hydraulic model is shown in Figure 11. The upstream reservoir, 3.0 m long and 3.0 m wide, was separated from the flood plain (3.75×3.0 m) by a dam of thickness $d = 0.12$ m. The obstacle and four selected gauges, which measured depths (at P1, P2, P3, P4), were located in the flood plain. Water can flow into the floodplain through a movable wall with a width of $D = 0.5$ m.

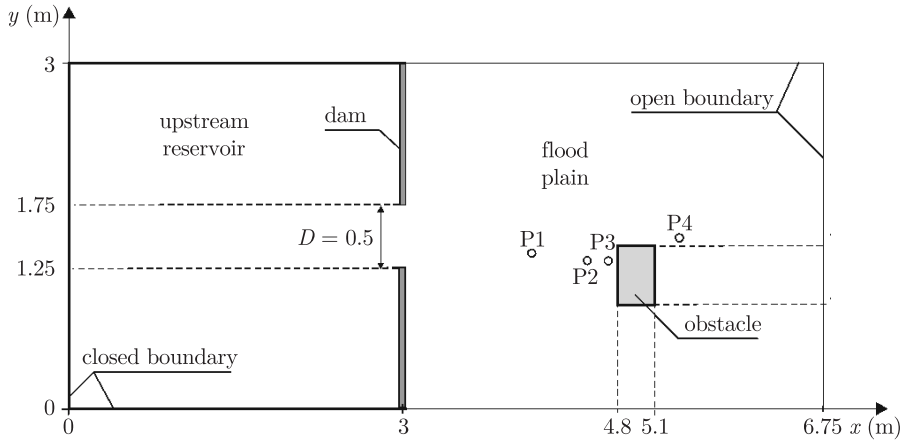

Figure 11. Geometry of the hydraulic model; deployment of the gauges P1 (4.15;1.40), P2 (4.55;1.30), P3 (4.75;1.30), P4 (5.40;1.50) (Szydłowski [24])

A constant value of the Manning roughness coefficient $n = 0.018\,\mathrm{m}^{-1/3}\mathrm{s}$ and zero bottom slope were assumed for the entire domain. At the initial time, the water body is at rest with the water depth $h = 0.21$ m in the upstream reservoir and a dry state with $h = 0.001$ m in the flood plain. At the closed boundary (the dam and obstacle), the unit discharge in the normal direction was set to zero. The laboratory experiment was reproduced using a numerical model. The calculations were carried out for a rectangular mesh $\Delta x = \Delta y = 0.05$ m with a time step of $\Delta t = 0.01$ s. The numerical solution in the form of depths is presented in Figure 12. Water levels before the obstacle are significantly increased and, at the same time, a hydrodynamic shadow characterized by small depths appeared behind the obstacle. Figure 13 shows a comparison between results of physical experiments and numerical calculations in the form of time series of depths. At points P1, P2 and P4, we obtained satisfactory agreement with numerical solutions, whereas in the vicinity of the obstacle (point P3), a significant discrepancy was observed.

6. Summary

We present the solution of the shallow water equations employed to simulate dam-break and dike-break induced flow. The numerical scheme of the finite volume method was based on the wave-propagation algorithm proposed by LeVeque [5]. In this approach, the numerical flux was computed by an approximate solution of

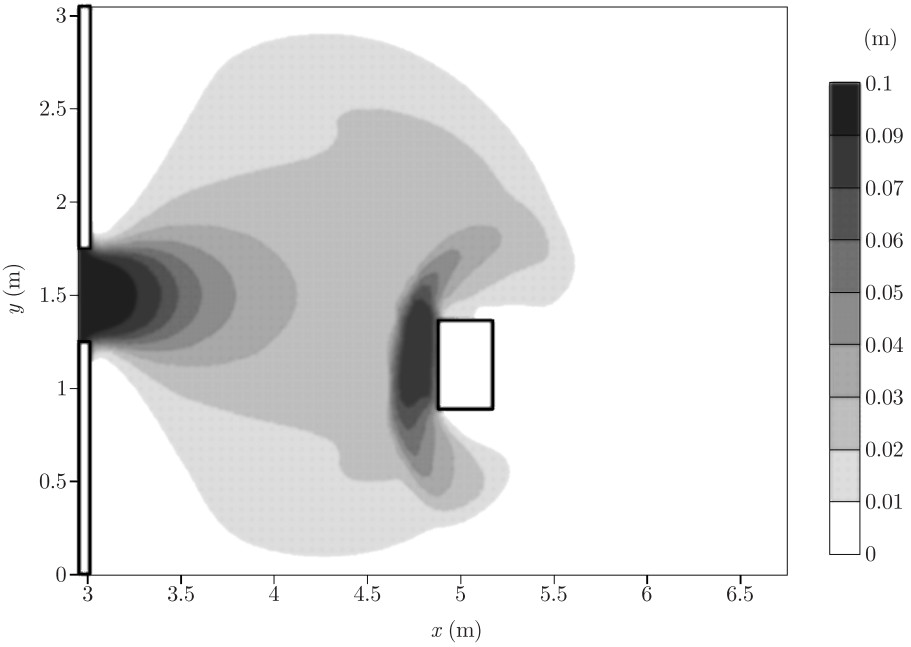

Figure 12. Depths at time $t = 2$s after the dam-break

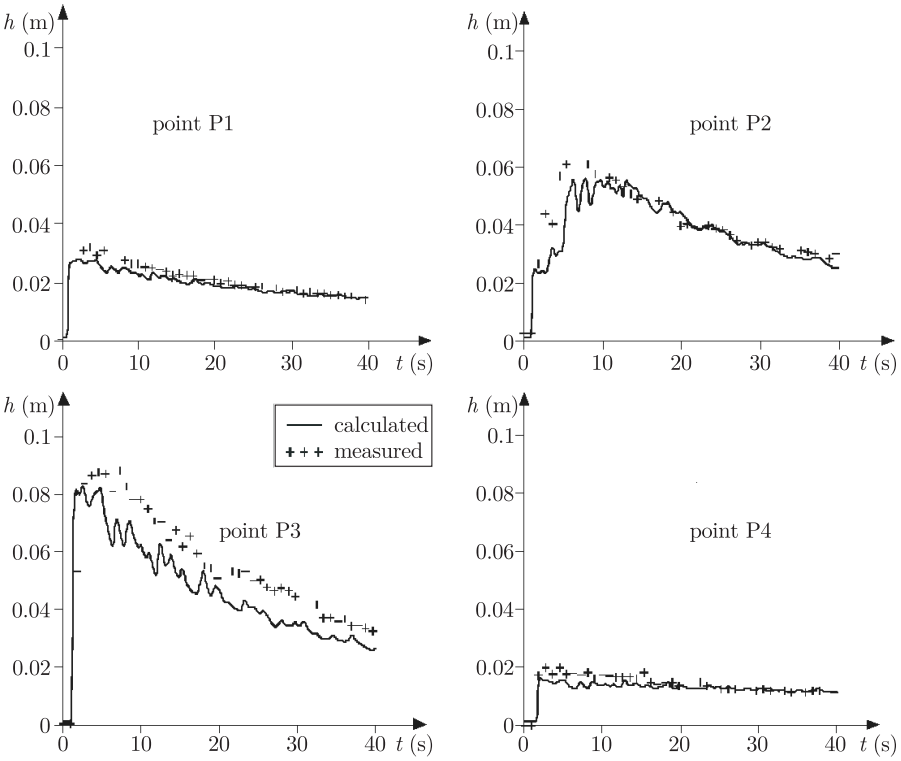

Figure 13. Comparison of measured and calculated depths at points P1, P2, P3 and P4

the Riemann problem, using the Roe method. The numerical scheme is second-order accurate in time as well as in space for a smooth solution. A stable solution without oscillations near the discontinuity (the front of the shock wave) was obtained by means of an appropriate correction of the numerical flux using the Van Leer limiter functions. The applied dimensional splitting according to the directions (x and y) leads to an effective algorithm, and, together with the wave-propagation algorithm, ensures the proper incorporation of the bottom source term into the scheme of the finite volume method. The splitting with regard to the friction processes additionally ensures a suitable approximation of the friction term during the simulation of supercritical flow.

The presented algorithm was validated on a number of numerical test cases. The obtained numerical results showed good agreement with the analytical solution of the one-dimensional case, and the physical experiments confirmed that the simulation of flows was accurate in the case of the two-dimensional dam-break and dike-break problems.

References

[1] Cunge J A, Holly Jr F M and Verwey A 1980 *Practical Aspects of Computational River Hydraulics*, Pitman, London
[2] Tan Weiyan 1992 *Shallow Water Hydrodynamics*, Elsevier, Amsterdam
[3] Szymkiewicz R 2010 *Numerical Modeling in Open Chanel Hydraulics*, Springer
[4] Toro E F 1997 *Riemann Solvers and Numerical Methods for Fluid Dynamics*, Springer-Verlag, Berlin
[5] LeVeque R J 2002 *Finite Volume Methods for Hyperbolic Problems*, Cambridge University Press
[6] Glaister P 1988 *J. Hydraul. Res.* **26** (3) 293
[7] Snaders B F 2001 *J. Hydraul. Res.* **39** (3)
[8] Nujic M 1995 *J. Hydraul. Res.* **33** (1) 101
[9] Mingham C G and Causon D M 1998 *J. Hydraul. Engng* **124** (6) 605
[10] Szydłowski M 2001 *Arch. Hydro-Engng Environ. Mech.* **XLVIII** (1) 35
[11] Aureli F and Mignosa P 2002 *Rapidly Varying Flows Due to Levee-Breaking*, *River Flow 2002, Proc. First Int. Conf. on Fluvial Hydraulics*, Louvain La Neuve, Belgium (Bousmar D and Zech Y, Eds.)
[12] Liang Q, Borthwick A G and Stelling G 2004 *Int. J. Num. Meth. in Fluids* **46** 127
[13] Roger S, Dewals B J, Erpicum S, Schwanenberg D, Schüttrumpf H, Köngeter J and Piroton M 2009 *J. Hydraul. Res.* **47** (3) 349
[14] LeVeque R J 1997 *J. Comput. Phys.* **131** 327
[15] Bale D S, LeVeque R J, Mitran S and Rossmanith J A 2002 *SIAM, J. Sci. Comput.* **24** (3) 995
[16] Szymkiewicz R 1993 *J. Hydraul. Engng* **119** (10) 1118
[17] Roe P L 1981 *J. Comput. Phys.* **43** 357
[18] Fletcher P S 1991 *Computational Techniques for Fluid Mechanics*, Springer Verlag, Berlin
[19] Bermudez A and Vazquez M E 1994 *Computers and Fluids* **23** 1049
[20] Garcia-Navarro P and Vazquez-Cendon M E 2000 *Computers and Fluids* **29** 951
[21] Stoker J J 1957 *Water Waves*, Interscience Publishers
[22] Wu C, Huang G and Zheng Y 1999 *J. Hydraul. Engng* **125** (11) 1210
[23] Fennema R J and Chaudhry M H 1990 *J. Hydraul. Engng* **116** (8) 1013
[24] Szydłowski M 2007 *Modelling of Flood Waves in Urban Areas*, Gdansk University of Technology (in Polish)